Inorganic Chemistry

Article

pubs.acs.org/IC

Chemical Bond Characterization of a Mixed-Valence Tri-Cobalt Complex, $Co_3(\mu\text{-admtrz})_4(\mu\text{-OH})_2(CN)_6\cdot 2H_2O$

Lai-Chin Wu,[†,⊥] Tsu-Chien Weng,[‡,$] I-Jui Hsu,*[,§] Yi-Hung Liu,[#] Gene-Hsiang Lee,[#] Jyh-Fu, Lee,[∥] and Yu Wang*[,†,#]

[†]Department of Chemistry, National Taiwan University, Taipei, Taiwan

[‡]European Synchrotron Radiation Facility, Grenoble Cedex, France

[§]Department of Molecular Science and Engineering, National Taipei University of Technology, Taipei, Taiwan

[#]Instrumentation Center, National Taiwan University, Taipei, Taiwan

[∥]National Synchrotron Radiation Research Center, Hsinchu, Taiwan

Supporting Information

ABSTRACT: Charge density study of a mixed-valence tri-cobalt compound, $Co_3(\mu\text{-admtrz})_4(\mu\text{-OH})_2(CN)_6\cdot 2H_2O$ (**1**) (admtrz = 3,5-dimethyl-4-amino-1,2,4-triazole), is investigated based on high resolution X-ray diffraction data and density functional theory (DFT) calculations. The molecular structure of this compound contains three cobalt atoms in a linear fashion, where two terminal ones are Co^{III} at a low-spin (LS) state and a central one is Co^{II} at a high-spin (HS) state with a total spin quantum number, S_{total}, of 3/2. It is centrosymmetric with the center of inversion located at the central Co atom (Co2). The Co2 ion is linked with each terminal cobalt (Co1) ion through two μ-admtrz ligands and a μ-OH ligand in a CoN_4O_2 coordination, where the Co1 is bonded additionally to three CN ligands with CoN_2OC_3 coordination. The combined experimental and theoretical charge density study identifies the different characters of two types of cobalt ions; more pronounced charge concentration and depletion features in the valence shell charge concentration (VSCC) are found in the Co^{III} ion than in the Co^{II} ion, and d-orbital populations also show the difference. According to topological properties associated with the bond critical point (BCP), the Co1−C(N) bond is the strongest among all the Co-ligand bonds in this compound; the Co−O is stronger than Co−N bond. Again Co1−O is stronger than Co2−O, so as the Co1−N being stronger than Co2−N bond. The electronic configuration of each type of Co atom is further characterized through magnetic measurement, Co-specific X-ray absorption near edge spectroscopy (XANES), and X-ray emission spectra (XES).

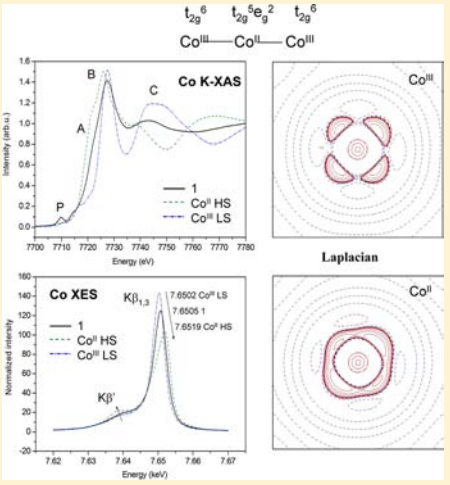

INTRODUCTION

Mixed-valence transition metal complexes have drawn a great deal of attention for a long time. The valence localization/delocalization character and intervalence charge transfer[1−3] of such mixed-valence complexes do provide a wide range of applications, such as in magnetic materials[4,5] and electrochromic materials.[6] Mixed-valence complexes are often found in multimetal centered coordination complexes. Some of these complexes are characterized as single molecule magnets (SMM),[7−9] single chain magnets (SCM),[10−12] and molecular metal wires.[13] For example, the well-known Mn mixed valent compound[14] $[Mn_{12}O_{12}(CH_3COO)_{16}(H_2O)_4]$ is a SMM with Mn^{III} and Mn^{IV} ions having an S_{total} of 8; another complex, $\{Mn_2(saltmen)_2Ni(pao)_2(py)_2\}(ClO_4)_2$ (saltmen^{2-} = *N*,*N*′-(1,1,2,2-tetra-methylethylene) bis(salicyl-idene iminate) and pao$^-$ = pyridine- 2-aldoximate),[10] is found to be the first SCM with a heterometallic chain of Mn^{III} and Ni^{II} ions with S_{total} = 3; the linear molecular metal wire of $\{Ni_5(bna)_4(Cl)_2\}(PF_6)_2$ (bna = binaphthyridylamide) is a mixed Ni^{II} and Ni^{I}.[13]

A thermal- and photoinduced reversible electron transfer phenomenon of a Fe_2Co trinuclear complex, $\{[FeTp(CN)_3]_2Co(Meim)_4\}\cdot 6H_2O$ (Tp = hydrotris(pyrazolyl)borate, Meim = *N*-methylimidazole) was reported[2] very recently with two terminal iron ions linked to a central cobalt ion through CN bridging ligands. The thermally induced electron transfer is observed to be accompanied with an abrupt spin transition between Fe^{III}_{LS}−CN−Co^{II}_{HS}−NC−Fe^{III}_{LS} state (S_{total} = 5/2) at 240 K and Fe^{II}_{LS}−CN−Co^{III}_{LS}−NC−Fe^{III}_{LS} state (S_{total} = 1/2) at 150 K. Such electron transfer process between cobalt and iron ions can also be induced by irradiation with 532 nm laser light at 5 K. Such electron transfer phenomenon is fully confirmed by magnetic susceptibility, ^{57}Fe Mossbauer spectra, UV−vis, IR X-ray diffraction, and absorption.[15−19]

The ligand 3,5-dimethyl-4-amino-1,2,4-triazole (admtrz) is an intriguing ligand, which may coordinate to metal atoms in

Received: May 16, 2013
Published: September 17, 2013

   dx.doi.org/10.1021/ic401147b | *Inorg. Chem.* 2013, 52, 11023−11033

various modes depending on the coordination site and the nature of the substituent. Such ligands serve as bridging ligand between two metal atoms through nitrogen atoms of the triazole ring. Many studies have established the magneto-structural correlations of transition metal complexes containing 1,2,4-triazole bridging ligands.[20−25] These compounds show quite different magnetic behaviors; some of them even exhibit spin crossover phenomena.[24−27] For example, the complex $[Fe(\mu\text{-atrz})(\mu\text{-pyz})(NCS)_2]$ atrz = 4,4′azo-bis-1,2,4-triazole, where the ligand, atrz, serves as a bridge between the octahedral coordinated Fe ions, gives rise to a spin transition with a wide hysteresis of 26 K (197−223 K).[25] Mixed valent compounds in linear tri-Mn complexes through admtrz linkage were found in a tri-Mn complex, $\{Mn_3(admtrz)_6(OH)_2(DMF)_2(H_2O)_2\}_2(ClO_4)_{10}\cdot(admtrz)_2\cdot 3H_2O$,[28] where three Mn ions are designated as $Mn^{II}-Mn^{III}-Mn^{II}$, with an antiferromagnetic coupling coefficient, J, of -4.47 cm^{-1}. Other than **1**, three tri-Co complexes, $(Et_4N)_4\{Co[Co(N_2(SO_2)_2)(CN)(OH)]_2\}$ (**2**),[29] $\{Co_3[(py)C(ph)NO]_6\}^{2+}$ (**3**),[30] and $\{Co_3[(py)C(H)NO]_6\}^{2+}$ (**4**),[30] are all found to be in $Co^{III}_{LS}-Co^{II}_{HS}-Co^{III}_{LS}$ state.

High resolution X-ray diffraction is a unique and useful tool for mapping the charge density distribution in crystals.[31−33] Electron density studies on 3d transition metal complexes have been reported[34−42] extensively for a couple of decades. Some studies have even involved 4d or 5d transition metal complexes[43−45] and on multinuclear complexes.[46−56] The basic properties derived from the charge density at the ground state have been thoroughly discussed.[31−42] Recent review articles[32,33] also lead to new directions of charge density analyses. Charge density studies of a light-induced metastable state have been reported,[57,58] where in the case of *cis*-$Fe(phen)_2(NCS)_2$ it[57] demonstrates the distinct differences in electron density distribution of Fe at high spin (HS) and at low spin (LS) state; the other example is on a $[Ni(NO)(\eta^5\text{-Cp}^*)]$ complex.[58] The topological properties are analyzed both in experimental and in theoretically calculated electron density based on Bader's "atoms in molecules: a quantum theory (QTAIM)".[59] Total electron density can be obtained experimentally from X-ray diffraction data in terms of multipole model (MM)[60] and theoretically calculated based on density functional theory (DFT) calculations. Bond characterizations such as bond type, bond strength, and localization/delocalization can then be classified according to the topological properties associated with the bond critical point (BCP),[32,61] together with source function[62] and Fermi-hole distributions.[63−65] Intermolecular interactions can be investigated through the Hirshfeld surface[66−68] and electrostatic potential.[59] A combined charge and spin density study from experimental X-ray diffraction data on a Yittrium complex was investigated.[44]

The X-ray absorption near edge spectroscopy (XANES) and X-ray emission spectra (XES) are both atom specific and are quite useful to characterize the exact electronic configuration of the target atom. The XANES is well established to identify the oxidation state and the local coordination environment of the target atom. The K-edge absorption spectra of 3d transition metal ions reveal a strong dependence on the charge distribution and on the coordination geometry of the metal site.[69] XANES spectroscopy of a series of the mixed valent perovskite $LaMn_{1-x}Co_xO_3$[70,71] provides a ratio of Co^{2+}/Co^{3+} and Mn^{3+}/Mn^{4+} in the compounds. High resolution Kβ XES is a straightforward way to explore the localized spin moment of 3d orbitals, thus the effective charge of 3d transition metal ions. The energy of Kβ line [3p → 1s] of such metal ions is quite sensitive to the spin states of 3d shell due to the strong exchange interaction between the 3p hole and the 3d electrons in the final state of the emission process.[72,73] This XES technique was successfully applied to examine the valence state of metal ions in a $La_{1-x}Ca_xMnO_3$ series,[74−76] in $(La,Sr)CoO_3$ under high pressure,[77] in magnetic transition under pressure,[78,79] and in some spin crossover systems.[77,80−82] Several techniques including magnetic property, X-ray absorption (XAS), XES, and charge density (CD) studies are presented in this work to verify the bonding characters as well as the electronic configurations of the metal ions of such a mixed-valence Co complex.

EXPERIMENTAL SECTION

Preparation of $Co_3(\mu\text{-admtrz})_4(\mu\text{-OH})_2(CN)_6\cdot 2H_2O$. Crystals of $Co_3(\mu\text{-admtrz})_4(\mu\text{-OH})_2(CN)_6\cdot 2H_2O$ (**1**) were prepared by mixing CoF_3 (23.18 mg, 0.2 mmol) and $CoCl_2$ (12.98 mg, 0.1 mmol) in 10 mL of water first, and adding admtrz (44.85 mg, 0.4 mmol in 10 mL of water) solution to the mixture. The KCN (39.07 mg, 0.6 mmol in 20 mL of water) solution was then slowly dripped into the previously prepared solution that was kept stirring. Pink powder precipitated as soon as the KCN solution was added; the solution was kept stirring slowly for 1 h. The pink solution after filtration was left still for a month before well-shaped pink crystals were obtained. A suitable single crystal was chosen for X-ray diffraction; powder samples used for XAS and XES were made by grinding the single crystals.

Data Collection and Refinement. High resolution X-ray diffraction data of **1** were collected using Oxford CCD diffractometer with a working power of 50 kV and 40 mA at 100 K with Ruby CCD detector. The crystal size is 0.12 × 0.15 × 0.25 mm, and the crystal to detector distance is 5.5 cm. Temperature is controlled using an Oxford CryojetXL liquid nitrogen device. Low and high angle data sets were taken at an exposure time of 5 and 50 s respectively with ω-scan width of 0.75°. Relative intensities were integrated through profile fitting individually. The absorption correction was applied according to the face measurements. Data collection and data reduction procedures were made using the CrysAlis program.[83] The resolution of the data is up to 1.06 Å^{-1} in $(\sin\theta)/\lambda$ with a completeness of 99.5%. The crystal structure of **1** was determined by direct method[84] and was refined by full-matrix least-squares based on F^2 of observed reflections ($I > 2\sigma(I)$) using SHELXTL program.[85] All non-hydrogen atoms were refined anisotropically. All H atoms (CH_3, NH_2, and OH) were obtained from a difference Fourier map. Crystal data of **1** are listed in Table 1 (details are provided in Supporting Information, Table S1). The final agreement indices of the spherical model are $R_1 = 0.0272$, $wR_2 = 0.0624$. The crystallographic data is deposited as CCDC-924142 in the Cambridge Crystallographic Data Centre (CCDC), which can be accessed via www.ccdc.cam.ac.uk/data_request/cif.

Multipole Model Refinement. The multipole model is applied based on the following equation:[60,61]

$$\rho_{atom}(r) = P_c\rho_{core}(r) + P_{val}\kappa^3\rho_{val}(\kappa r) + \sum_{l=0}^{l_{max}}\kappa'^3 R_l(\kappa' r)\sum_{m=0}^{l} P_{lm\pm}d_{lm\pm}(\theta,\phi); \qquad R_l(r)\frac{\alpha_l^{n_l+3}}{(n_l+2)!}r^{n_l}e^{-\alpha_l r}$$

The first two terms are the spherical part of atomic electron density; the third term describes the nonspherical part of the electron density, which is expressed as the sum of multipoles using the real part of spherical harmonic functions (Y_{lmp}); $R_l(r)$ is the radial function; κ and κ' serve as the expansion−contraction factor of the radial distribution. P_c and P_{val} is the population of core and valence electron respectively; P_{lm} is the coefficient of multipole term; all P_{lm} parameters and P_{val}, κ, κ' are obtained through the least-squares refinements using the XD2006[86] program. Two different electron configurations of the cobalt atoms were taken as $[Ar]3d^7$ for Co^{II} and $[Ar]3d^6$ for Co^{III} ions

dx.doi.org/10.1021/ic401147b | Inorg. Chem. 2013, 52, 11023−11033

Table 1. Crystal Data of 1 at 100 K

empirical formula	$C_{22}H_{42}Co_3N_{22}O_6$
formula weight	887.57
temperature	100(2) K
space group	$P2_1/c$
unit cell dimensions	a = 10.8274(1) Å
	b = 9.82110(8) Å
	c = 17.73730(2) Å
	β = 103.0260(8)°
volume, Z	1837.60(2) Å^3, 2
crystal size, mm	0.25 × 0.14 × 0.12
θ range for data collection	3.14−48.67° (sin θ/λ = 1.06)
reflections collected	153502
independent reflections	18076, R_{int} = 0.0450
completeness (%)	99.5
data/restraints/parameters	12653/0/336
final R indices[a] [$I > 2\sigma(I)$]	R_1 = 0.0272, wR_2 = 0.0624
R indices (all data)	R_1 = 0.0453, wR_2 = 0.0645
multipole refinement	
data/restraints/parameters	11374/63[b]/824 (sin θ/λ = 1.04)
final R indices [$I > 3\sigma(I)$]	R_1 = 0.0171, Rw = 0.0083
	R_2 = 0.0206, wR_2 = 0.0165

[a] $R_1 = \sum||F_o| - |F_c||/\sum|F_o|$; $R_{1w} = (\sum|F_o - F_c|^2/\sum w|F_o|^2)^{1/2}$; $R_2 = \sum|F_o^2 - F_c^2|/\sum|F_o^2|$. $wR_2 = \{\sum[w(F_o^2 - F_c^2)^2]/\sum[w(F_o^2)^2]\}^{1/2}$; $R_{int} = \sum[n/(n-1)]^{1/2}|F_o^2 - \bar{F}_o^2|/\sum F_o^2$. [b] Fixed position parameters of hydrogen atoms.

where [Ar] means Ar core with $3d^7$ or $3d^6$ as valence electrons. The single-ξ Slater type functions were taken from Clementi and Raimondi;[87,88] a better linear combination of Slater-type functions fitting of relativistic atomic wave functions[89] was also tried; it gave essentially the same density distribution. The spherical atomic scattering amplitudes were taken from International Tables for X-ray Crystallography.[90]

The atomic parameters (positional and thermal displacements) were first refined using high order data ((sin $\theta)/\lambda$ = 0.5−1.04 Å^{-1}); the multipole parameters were then refined based on F^2 of observed reflections ($F^2 > 3\sigma(F^2)$) of full data. The C−H distances were fixed at 1.08 Å according to the neutron data.[41,91] The internal coordinates of metal are defined as the z-axis along the Co−O1 direction and the x-axis at the bisecting direction of N−Co−N or C−Co−C angles (shown in Supporting Information, Figure S1)[38,39] in order to better correlate the d-orbital populations, though this is different from the definition of previous studies.[92,93] The multipole terms are included up to hexadecapole for Co, octapole for C, N, O atoms and dipole for H. The n_l value used are (4 4 4 4) for Co and (2 2 3) for C and N atoms. Two different κ parameters were applied to Co2 and Co1 ions. The κ' parameters were also included in the final refinement. The agreement indices after multipole refinement do improve significantly from the spherical model indicating the multipole model does fit better with the total electron density. Topological analyses were applied based on Bader's QTAIM theory.[59] The experimental total electron density, deformation density, Laplacian distributions and the topological properties associated with the BCPs were obtained using XD2006 program.[86] The corresponding DFT calculated ones were derived from the XAIM program.[94]

DFT Calculation. The theoretical calculated charge density is obtained from a single-point calculation based on the experimental geometry using the Gaussian03[95] program. Open-shell spin-unrestricted calculations were carried out with the spin multiplicity of 4. The open shell hybrid XC functional uB3LYP[96,97] is used with basis sets of 6-311+G* and 6-31G*, respectively, for Co and the rest of atoms. The natural bond orbital (NBO) analysis is applied using NBO 3.0,[98] and effective bond orders (eBO) are calculated accordingly.

XANES and XES. XANES at the Co K-edge was measured at beamline 17C at NSRRC (Hsin-Chu, Taiwan) with operational energy of 1.5 GeV and working current of 200 mA in top-up mode. A Si(111) double crystal monochromator was optimized to reach an energy resolution ($\Delta E/E$) of about 2 × 10^{-4}. Samples were ground evenly and glued on a tape before taking the measurements, gas ionization chamber was used to monitor the intensity of incident beam. All spectra were recorded in fluorescence mode by Lytle detector at room temperature. The energy calibration was made using cobalt metal foil (7709 eV).

XES of **1** and reference compounds were carried out at the ID26 beamline of the European Synchrotron Radiation Facility (ESRF). The radiation was monochromatized by a cryogenically cooled fixed-exit double-crystal monochromator, Si(311), the resolution power $\Delta E/E$ is ∼10^{-4}. The incident beam is focused to a size of 300 μm (horizontal) × 100 μm (vertical) at the sample position using the biomorph K−B system. The sample (S), the analyzer (A), and the detector (D) were arranged on a 1 m in diameter Rowland-circle spectrometer. A spherically bent Si(533) crystal (analyzer) and an Avalanche Photodiode (APD) were applied to analyze and detect the emitted radiation respectively. The K$\beta_{1,3}$ and Kβ' emission lines were measured in the range 7.62−7.67 keV. The step size of energy scan is 0.4 eV. XAS and XES can provide the direct information of charge and spin state of cobalt ions in complex **1**. In order to get the proper information of charge and spin state of cobalt ions in complex **1**, compounds with known charge and spin state, $[Co^{II}(phen)_3](ClO_4)_2$ and $K_3[Co^{III}(CN)_6]$, are prepared as the reference of Co^{II}_{HS} and Co^{III}_{LS}, respectively.

RESULTS AND DISCUSSION

Structure Description. Compound **1** is crystallized in a monoclinic space group $P2_1/c$ with Z = 4. The molecular structure is displayed in Figure 1. It consists of three Co atoms

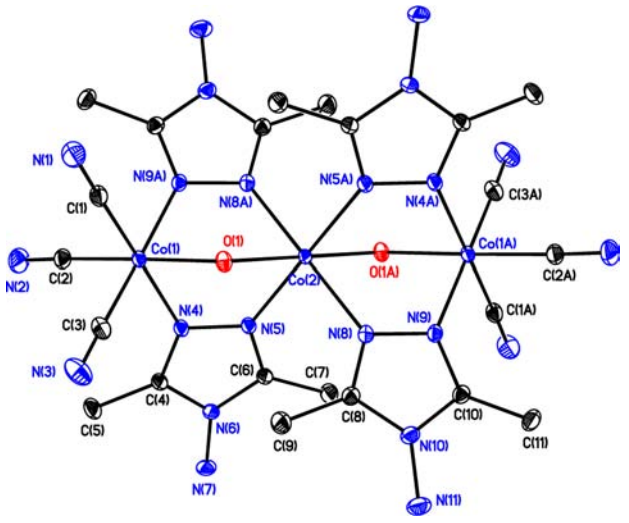

Figure 1. Molecular structure of $Co_3(\mu\text{-admtrz})_4(\mu\text{-OH})_2(CN)_6\cdot 2H_2O$ (**1**) at 100 K drawn with 50% probability in thermal ellipsoids.

arranged in a linear fashion with Co···Co distance of 3.275(1) Å. The central Co atom (Co2) is located at the center of inversion; the terminal Co (Co1) and the central Co2 are bridged by four μ-admtrz ligands and two μ-hydroxo (OH^-) ions; three additional CN ligands are coordinated to Co1; thus both Co atoms are in distorted O_h geometry with CoN_2OC_3 and CoN_4O_2 for the coordination of Co1 and Co2, respectively. Two water molecules are located in the lattice; one of them is in disordered model with 60/40% occupancies in O atoms; however, only two H atoms are located yet they give reasonable geometries connecting both O atoms (∠H−O−H of 94 and 101°; O−H distance of 0.8−0.9 Å). There are

dx.doi.org/10.1021/ic401147b | Inorg. Chem. 2013, 52, 11023−11033

H-bonds between water molecule, hydroxide, N_{CN} and N_{trz} of the admtrz ligand, listed in the Supporting Information, Table S6. Selected bond distances around Co metal ions are listed in Table 2, together with those of compounds **2**, **3**, and **4**. The

Table 2. Selected Bond Distances (Å) and Distortion Parameters (Σ) of Tri-Cobalt Mixed-Valence Complexes ($Co1^{III}\cdots Co2^{II}\cdots Co1^{III}$)

	1	**2**[29]	**3**[30]	**4**[30]
	$P2_1/c$	$C2/c$	$P\bar{1}$	$R\bar{3}$
temp (K)	100	100	298	298
formal charge	III,II,III	III,II,III	III,II,III	III,II,III
spin state	LS,HS,LS	LS,HS,LS	LS,HS,LS	LS,HS,LS
Co···Co	3.275(1)	3.677(3)	3.464(4)	3.466(2)
	X = N	X = O	X = O	X = O
$Co2^{II}$–X	2.1224(5)	2.088(3)	2.104(2)	2.102(2)
	2.1310(5)			
$Co2^{II}$–OH	1.9949(4)	2.015(3)		
$Co1^{III}$–N	1.9963(5)	1.991(3)	1.952(2)	1.961(2)
	2.0018(5)			
$Co1^{III}$–OH	1.9049(4)	1.940(3)		
$Co1^{III}$–CN	1.8546(6)	1.876(3)		
	1.8820(6)			
	1.8597(7)			
Σ(Co1)	27.79°	28.80°	49.69°	47.70°
Σ(Co2)	70.81°	47.68°	18.04°	2.40°

Co–N bond distances are 1.9963(5) Å and 2.0018(5) Å for Co1 and 2.1224(5) Å and 2.1310(5) Å for Co2, which indicates that Co1–N is 0.12 Å shorter than Co2–N. Similarly, the bond distance of Co1–O, 1.9049(4) Å is 0.087 Å shorter than that of Co2–O, 1.9949(4) Å. The average Co1–C bond distance is 1.865 Å. Bond distances around Co1 and Co2 are provided in Supporting Information (Table S2). The degree of distortion from ideal octahedral geometry is defined by a parameter, Σ,[99,100] which is the sum of the 12 L–M–L angles deviated from the value of 90 deg. This parameter listed in Table 2 indicates that it is far more distorted in Co2 than in Co1, with a respective Σ value of 70.81° and 27.79°. Accordingly, the bond distance of Co2–L is longer than that of Co1–L, which is comparable with those found in related compounds **2**–**4**[29,30] tabulated in Table 2. In comparison with all these tri-Co compounds, the Co···Co distance of **1** (3.285 Å) is significantly shorter than those of the others (longer than 3.4 Å); this may be due to the shorter Co–O distance of **1**. According to the distortion parameter (Σ), the cobalt(III) site is closer to a regular octahedron than that of cobalt(II) in **1** and **2**. It shows the opposite for **3** and **4**; however, the ligand of central Co in **3** and **4** is in a more open and flexible binding mode. Therefore, it gives a rough octahedral environment; the ligand of the terminal Co is, on the other hand, a constrained tridentate one, which gives a distorted O_h environment. Thus, it is not a fair comparison of Σ for the difference in the spin state of **3** and **4**.

Compound **2**[29] has been identified as $Co^{III}{}_{LS}$–$Co^{II}{}_{HS}$–$Co^{III}{}_{LS}$ by EPR spectroscopy and magnetic susceptibility. The coordination geometries of cobalt ions in **1** and **2**,[29] such as bond distances and distortion in O_h, are very similar to each other. Therefore, according to the Co–L bond distances, the electronic configurations of Co ions in compound **1** are likely to be the same as in **2**, i.e., $Co^{III}{}_{LS}$–$Co^{II}{}_{HS}$–$Co^{III}{}_{LS}$. Furthermore, the electronic configurations of Co ions in $\{[FeTp(CN)_3]_2Co(Meim)_4\}\cdot 6H_2O$[2] can be switched between $Co^{II}{}_{HS}$ and $Co^{III}{}_{LS}$ thermally or by photo irradiation, where the bond distance of $Co^{II}{}_{HS}$–N_{Meim} ≈ 2.12 versus $Co^{III}{}_{LS}$–N_{Meim} ≈ 1.967 Å and $Co^{II}{}_{HS}$–NC = 2.154 versus $Co^{III}{}_{LS}$–NC = 1.915 Å. On the basis of the Co–N distances of **1**, the Co1 should be assigned as Co^{III} at LS and Co2 as Co^{II} at HS.

Magnetic Property. The temperature-dependent magnetic susceptibility ($\chi_m T$) of **1** is depicted in Figure 2a. The $\chi_m T$

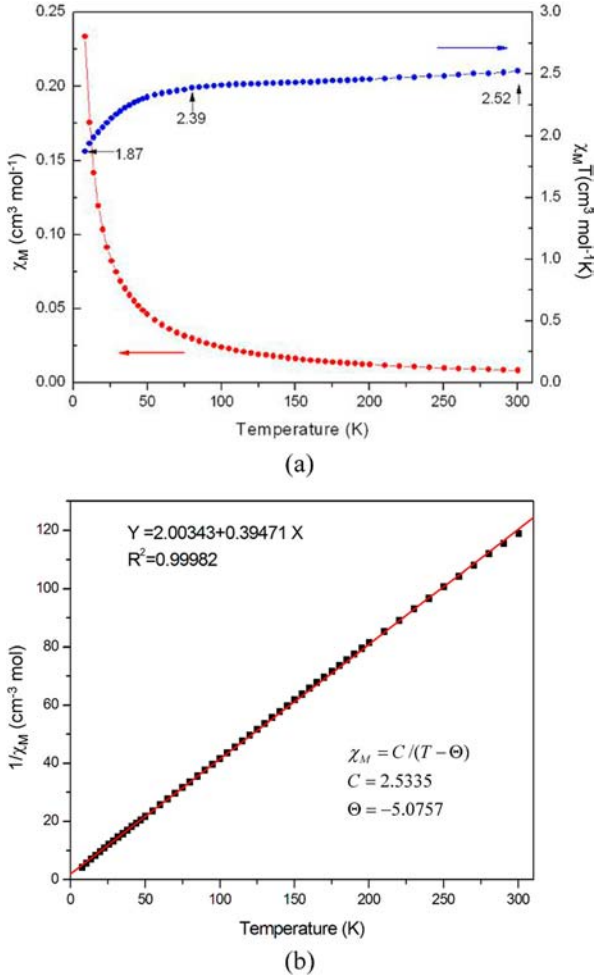

Figure 2. Plots of (a) χ_M (blue circles) and $\chi_M T$ (red circles) vs T and (b) $1/\chi_M$ vs T. The red line in (b) is the fitting curve according the Curie–Weiss equation: $\chi_M = C/(T - \Theta)$.

value slowly drops from 2.52 at 300 K to 2.39 at 80 K, which is much higher than the spin-only value of 1.875 for $Co^{II}{}_{HS}$ (S = 3/2), however taking the orbital contribution[29] into account as normally found in cobalt(II) complex at HS, which is in the range of 2.42–3.13.[101] As temperature is lowered below 80 K, the $\chi_m T$ further drops to 1.87 ($cm^3\ mol^{-1}\ K$) at 8 K, which is similar to that of **2**. It is interpreted as the combined effects of spin–orbital coupling and zero-field splitting.[29] The $1/\chi_M$ is fitted according to the Curie–Weiss equation, $\chi_M = C/(T - \Theta)$, shown in Figure 2b, which yields a Curie constant, C, of 2.5 and Θ of −5.1.

X-ray Absorption Near-Edge Structure (XANES). The XANES of **1** together with the reference compounds $[Co^{II}(phen)_3](ClO_4)_2$ of Co^{II} at HS ($t_{2g}{}^5e_g{}^2$) and $K_3[Co^{III}(CN)_6]$ of Co^{III} at the LS ($t_{2g}{}^6e_g{}^0$) state are displayed in Figure 3. The XANES of Co^{II} compound at HS (green) gives a strong absorption peak (white line) at ~7725 eV, which is

dx.doi.org/10.1021/ic401147b | Inorg. Chem. 2013, 52, 11023–11033

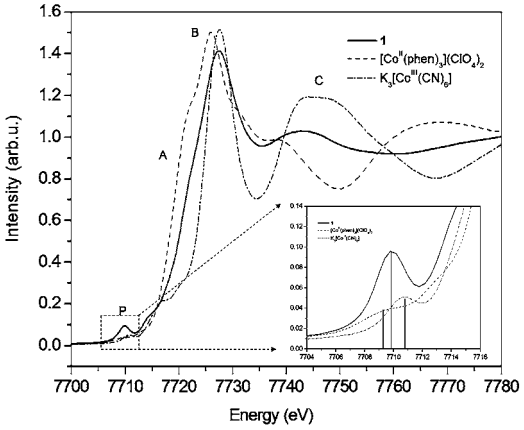

Figure 3. The Co K-edge XANES spectra of **1** (black line), $[Co^{II}(phen)_3](ClO_4)_2$ (dash green line), and $K_3[Co^{III}(CN)_6]$ (dash dot blue line). The inset is the enlarged part of the pre-edge region.

generally assigned as 1s → 4p allowed dipolar transition. The pre-edge peak at ~7709 eV is assigned to be 1s → 3d transition including 1s → e_g and 1s → t_{2g}. This absorption is through both quadrupolar transition and dipolar transition (p−d mixing).[102] An enlarged diagram of the pre-edge region is shown in the inset of Figure 3, and the intensity of such 1s → 3d transition is proportional to the unoccupied states of 3d orbitals.[102] However, due to the limitation of optical resolution, the double peaks (1s → e_g and 1s → t_{2g}) are not resolved so that only one peak around 7709 eV is observed for $Co^{II}(phen)_3(ClO_4)_2$. As for that of Co^{III} at the LS state, a pre-edge peak at ~7711 eV is observed which corresponds to 1s → e_g transition, and its white line is at ~7728 eV. Accordingly, the K-edge spectrum of Co^{III} shifts significantly to higher energy than that of Co^{II}, including the apparent peak positions of pre-edge, the rising edge regions, and the white line positions. The XANES of **1** shows a strong pre-edge absorption at ~7710 eV and the edge absorption at ~7727 eV. Both are between the values of Co^{II} and Co^{III} compounds. Thus, compound **1** is a mixed-valence compound with Co^{II} and Co^{III}.

X-ray Emission Spectrum. The XES of **1** and reference compounds ($[Co^{II}(phen)_3](ClO_4)_2$ and $K_3[Co^{III}(CN)_6]$) are depicted in Figure 4. The Kβ emission manifold shows in two main components an intense line and a broad satellite feature at lower energy side, which is due to the strong exchange interaction between the 3p hole and the 3d electrons.[103] The spectrum of Co^{II} compound gives a relatively lower intensity of K$\beta_{1,3}$ peak at 7615.9 eV and stronger satellite peak Kβ'. On the contrary, Co^{III} compound gives stronger K$\beta_{1,3}$ at 7650.2 eV and weaker Kβ' peak. These variations in the emission spectra of Co^{II} and Co^{III} compounds have been reported elsewhere.[81] Obviously, the XES of **1** gives features between those of Co^{II} and Co^{III} compounds shown in Figure 4a. When a simulated spectrum is derived from a linear combination with one-third of Co^{II} and two-third Co^{III} reference spectra, it agrees quite well with the spectrum of **1**. In order to show this clearly, the contribution of 1/3 Co^{II} is subtracted from the spectrum of **1**, the difference spectrum fits the 2/3 Co^{III} reference spectra quite well as shown in Figure 4b; only a slight shift of 0.4 eV is found in a peak position, which is within the standard deviation, corresponding to the step size of the measurement. Other ratios between two Co ions have been tried and give a not so good fit to the measured spectrum shown in Supporting Information, Figure S2b. The linear relationship between the average spin

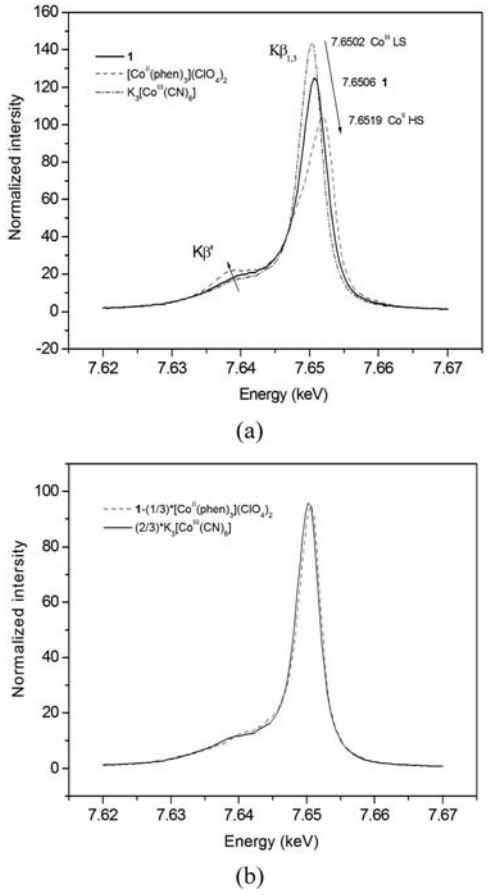

Figure 4. (a) K$\beta_{1,3}$ and Kβ' X-ray emission spectroscopy of **1** (black line), $[Co^{II}(phen)_3](ClO_4)_2$ (dash green line), and $K_3[Co^{III}(CN)_6]$ (dash dot blue line). The arrows indicate the direction of peak-maxima shift in Kβ'. (b) The difference spectra (dash red line) obtained by subtracting (1/3)*$[Co^{II}(phen)_3](ClO_4)_2$ from **1** and comparing it with (2/3)*$K_3[Co^{III}(CN)_6]$) (black line).

value and integrals of spectra area was established.[80,81] The integrals of absolute values of the difference spectra (IAD) introduced by György Vankó[80,81] is applied according to

$$IAD_i = \int |SP_i - SP_{ref}|\, dE$$

where SP_i and SP_{ref} are the intensities of the compound in interest and reference compound, respectively. This value is a promising indicator for estimating spin state of a metal ion due to its linear relationship with spin state of a metal ion. It is necessary to choose proper reference spectra of known spin states of atoms. Then, use the combination of those spectra to simulate the spectra.[81] The average spin values can be derived directly from the Kβ XES as well. Since the 3p → 1s emission is sensitive mainly to the effective spin of 3d, the average spin of the transition metal ion can be determined from the shape and position of the emission line.[73] When the assumed linear relationship between IAD values and average spin values of reference compounds is drawn, the value of **1** is very close to the point of the calculated (1/3 Co^{II} + 2/3 Co^{III}) value, with the average spin value of 1/2 for compound **1** (shown in Supporting Information, Figure S3).

Charge Density — Multipole Model (MM). The final agreement indices of multipole refinement are listed in Table 1. The MM is apparently well fitted to the experimental data with

dx.doi.org/10.1021/ic401147b | Inorg. Chem. 2013, 52, 11023−11033

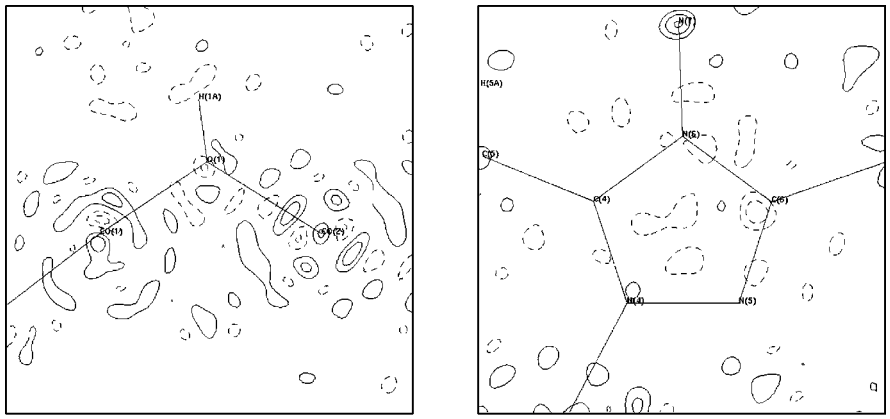

Figure 5. Residual density maps drawn from data up to 1.04 Å^{-1} with $F^2 \geq 3\sigma(F^2)$ at (a) Co1−Co2−O1 plane and (b) N4−N5−N7 plane. The contour interval is 0.1 e/Å^3; solid line positive and dotted line negative.

good agreement indices (R_1 = 0.0171, wR_2 = 0.0165) including 824 parameters based on 11 374 observed reflections ($F^2 > 3\sigma(F^2)$). The residual density from the MM (shown in Figure 5) shows nearly featureless everywhere in the molecule except around Co atoms; however, such residuals disappear when the reflections are included only up to $(\sin\theta)/\lambda$ of 1.04. A Hirshfeld rigid bond analysis gives the differences of mean-squares displacement amplitudes (DMSDA) of 10^{-4} and 10^{-3} for Co and ligand (N, O, C) related bonds. The complete list is given in the Supporting Information, Table S3.

The selected deformation density and Laplacian maps of admtrz are shown in Figure 6. The deformation density map is

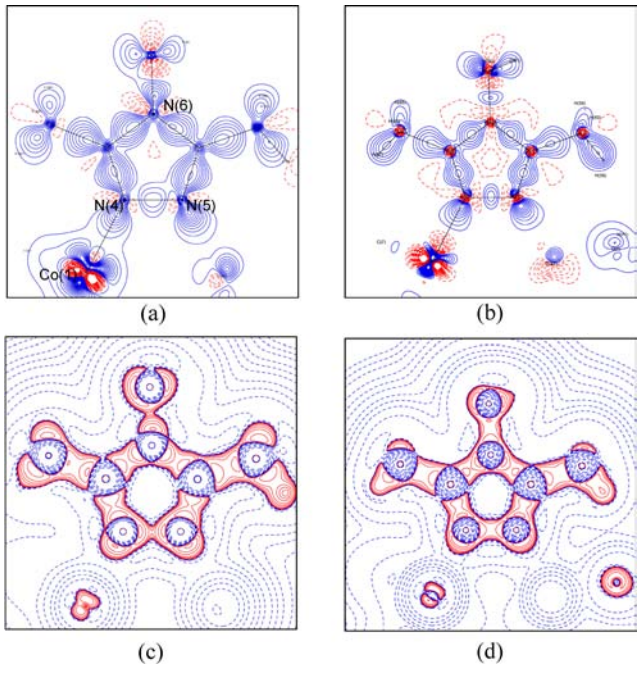

Figure 6. (a, b) Deformation density maps and (c, d) Laplacian maps of the admtrz ligand. The results of MM and DFT are shown in left (a, c) and right (b, d) column, respectively. The contours of deformation density map are 0.1 e/Å^3 with solid blue line positive and dotted red line negative. Laplacian distributions are plotted as $(-1)^l \times 2^m \times 10^n$ e/Å^5 (l = 0 or 1, m = 1−3, n = −3 to 3) with solid red line negative and dotted blue line positive.

the difference density between the MM and the independent atomic model (IAM). The deformation density accumulation is observed in every bonding region of the ligand. Local density accumulation is also observed (Figure 6a,b) at each lone pairs of the coordinated nitrogen atoms (N4, N5, N8, and N9) and carbon atoms (C1, C2, and C3); such accumulation is always pointed toward the density depletion region of the metal atom, which is in accord with the concept of donor−acceptor ligand−metal bond; similar observations were found in other metal complexes.[34−43,46−56]

The corresponding Laplacian distributions shown in Figure 6c,d give the same feature. The experimental and theoretical Laplacian distributions are in good agreement. The local charge concentration (LCC) can be observed around every C/N atom of the admtrz ligand in the bonding direction and at the lone pairs to form a triangular shape, as expected from sp^2 hybrid orbital. Likewise, two LCCs are found at each end of the CN ligand, a sp hybrid, as illustrated in the Supporting Information, Figure S5. This agrees exactly with the prediction of the valence shell electron pair repulsion (VSEPR) model.[104]

The deformation density maps of two cobalt ions at different coordination planes are shown in Figure 7. The asphericity in density distribution around Co is clearly shown as the expected donor−acceptor bond type; it also represents the uneven population of valence electrons among five 3d orbitals of the metal ion.[37,54,55] The corresponding Laplacian distributions at three unique planes shown in Figure 8a−d clearly show that LCC and local charge depletion (LCD) around the Co ion are in its fourth quantum shell of 3d valence shell charge concentration (VSCC). However, the valence shell of Co1 shows more distinct LCC and LCD than those of Co2, indicating the preferred population on t_{2g} than e_g orbital, where the crystal field splitting is manifested. Again electronic configuration of Co2 and Co1 is illustrated as $t_{2g}^5e_g^2$ and $t_{2g}^6e_g^0$, respectively.

Chemical Bond Characterizations and Topological Properties. The molecular graph drawn with bond critical points and bond paths are provided in Supporting Information, Figure S6. The positions of BCPs of all M−L bonds and N−N bonds of triazole five-membered ring are located at the mid point between two bonded atoms; those of C−N bonds are closer to the carbon atom. The selected experimental and theoretical topological properties at BCPs are listed in Table 3.

dx.doi.org/10.1021/ic401147b | Inorg. Chem. 2013, 52, 11023−11033

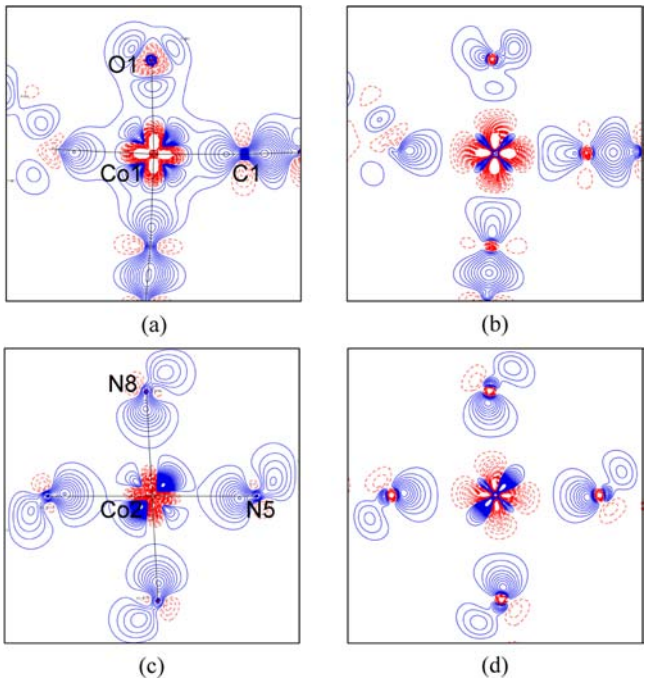

Figure 7. The experimental (a, c) and theoretical (b, d) deformation maps at the plane of (a, b) Co1−C1−O1, (c, d) Co2−N5−N8; the contours are defined as in Figure 6.

The full lists of topological properties of **1** are given in Supporting Information, Table S4.

The metal atoms in compound **1** are coordinated by three types of atoms: C, N, and O. All Co−X (X = O, N) bonds have similar topological properties at BCPs with 0.4−0.7 e Å^{-3} in ρ_b, positive $\nabla^2\rho_b$ and close to zero value in H_b. They can be characterized as polarized covalent bonds.[34−43,46−56] However, differences are observed between Co1−X and Co2−X; all Co1−X bonds have larger ρ_b than those of Co2−X, e.g., 0.73 vs 0.55 e Å^{-3} for Co−O bond; 0.63 vs 0.43 e Å^{-3} for Co−N bond, which are expected for a stronger bond with Co^{III} than with Co^{II}. In addition, a relative large ρ_b of 0.94 e Å^{-3} and a negative H_b of −0.3 HÅ^{-3} are found in the cobalt cyanide bond, Co1−C(N), indicating that this bond has a stronger covalent character than other M−L bonds. The topological properties associated with the BCPs of all Co−L bonds are comparable to those of other related metal−ligand interactions indicating donor−acceptor type, i.e., dative bond characters.[34−43,46−56]

A series of Cr−L bond studies with different types of nitrogen ligand was reported.[38] According to topological properties both from experiment and theory, the ρ_b values of Cr−N bonds are in the range of 1.87−0.54 e Å^{-3} with the value in the order of $Cr-N_{nitrido} > Cr-N_{imido} > Cr-N_{amido} > Cr-N_{pyridyl} \cong Cr-N_{pyrrole}$. The ρ_b value of $Co1-N_{trz}$ is slightly less than that of $Cr-N_{amido}$ but that of $Co2-N_{trz}$ is slightly less than that of $Cr-N_{pyridyl}$ as listed in Table 3. Therefore, the ρ_b value of Co−N of **1** is in the order $Cr-N_{amido} > Co1-N_{trz} > Cr-N_{pyridyl} > Co2-N_{trz}$. Among the M−O bonds, the type of oxygen can be H_2O,[37] OH^- (hydroxide) (**1**), O^{2-} (oxo)[38] or carboxylate[40] ligands. The $Cr-O_{oxo}$ bond[38] was confirmed as a metal−ligand multiple bond with ρ_b of 1.83 and H_b value of −1.24. The ρ_b value of Co1−O (0.729 e Å^{-3}) in **1** is definitely larger than those of carboxylate[40] or water ligand in $M(C_4O_4)(H_2O)_4$[37] with $\rho_b \approx 0.4$ e Å^{-3}.

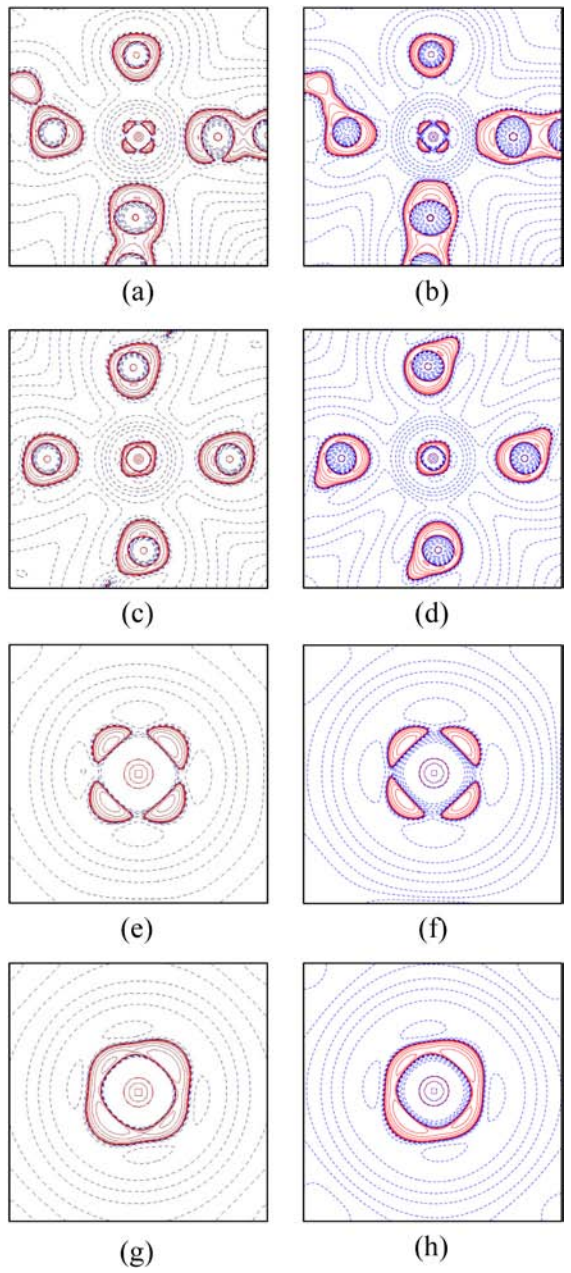

Figure 8. The experimental (a, c, e, g) and theoretical (b, d, f, h) Laplacian distributions plotted at the plane of (a, b) Co1−C1−O1 and (c, d) Co2−N5−N8. The plots (e−h) are the enlarged part of Co atoms on the same planes of (a−d). The contours are defined as in Figure 6.

The M−L multiple bond has been illustrated by Fermi-hole distribution[38] consisting of σ and π bond characters. The cyanide (CN^-) and carbonyl (CO) are known to be strong ligands due to its σ-donor and π-acceptor characters. The ρ_b value of Co−C bond is similar to other metal carbonyls, e.g., Co−C(O)[50] (bond distance (d) = 1.79 Å, ρ_b = 0.93 e Å^{-3} and H_b = −0.43 HÅ^{-3}) and Mn−C(O)[47] bonds ($d \approx 1.85$, $\rho_b \approx 0.89$ e Å^{-3} and $H_b \approx -0.34$ HÅ^{-3}) and to some metal carbene/carbyne bond, i.e., $Cr-C_{carbene}$[38] (d = 1.999 Å, ρ_b = 0.68 e Å^{-3}); $Cr-C_{carbyne}$[38] (d = 1.725 Å, ρ_b = 0.86 e Å^{-3}).

The C−N bond is a typical triple bond with ρ_b and H_b values of 3.5 e Å^{-3} and −5.76 HÅ^{-3} as well as a large negative $\nabla^2\rho_b$. Other intraligand bonds, N−N, C−C, and C−N, are also all in

dx.doi.org/10.1021/ic401147b | Inorg. Chem. 2013, 52, 11023−11033

Table 3. Selected Topological Properties Associated with Bond Critical Points of 1 from (a) MM and (b) DFT

bond distance (Å)		d_1[a] (Å)	ρ_b (e Å^{-3})	$\nabla^2\rho_b$ (e Å^{-5})	H_b (HÅ^{-3})
Co1−C1	a	0.934	0.929(8)	10.41(1)	−0.26
1.8546(6)	b	0.902	0.924	8.591	−0.38
Co1−N4	a	0.978	0.627(4)	9.570(3)	−0.05
1.9963(5)	b	0.932	0.555	10.837	−0.08
Co2−N5	a	1.031	0.441(3)	7.967(2)	0.03
2.1224(5)	b	1.007	0.439	6.562	−0.09
Co1−O1	a	0.945	0.729(4)	12.860(4)	−0.07
1.9949(4)	b	0.905	0.644	14.341	−0.04
Co2−O1	a	0.988	0.545(3)	10.934(4)	0.02
1.9949(4)	b	0.968	0.524	9.762	−0.07
C1−N1	a	0.464	3.64(3)	−53.0(2)	−5.76
1.1573(8)	b	0.395	3.176	5.781	−5.70
C4−N4	a	0.542	2.66(3)	−31.7(1)	−3.54
1.3233(7)	b	0.464	2.435	−25.039	−4.11
N4−N5[b]	a	0.691	2.36(2)	−4.06(5)	−2.78
1.3823(7)	b	0.690	2.344	−15.235	−2.29
N6−N7[c]	a	0.766	2.19(2)	−1.66(7)	−2.74
1.4015(7)	b	0.729	2.186	−14.035	−2.03
C4−C5	a	0.874	1.80(2)	−16.52(8)	−1.88
1.4788(8)	b	0.818	1.762	−15.385	−1.62

[a] d_1, distance of BCP from the first atom of the bond. [b] trz five-membered ring. [c] Amino group.

covalent character with a ρ_b value of 1.8−2.7 eÅ^{-3} and H_b value of −1.9 to −3.5 HÅ^{-3}, which indicates a delocalized double bond character in the five-membered ring.

The NBO analysis of metal−ligand bonds are listed in Table 4. The Co1−C bond gives an effective bond order of 0.9 with 37% contribution from Co spd hybrid orbitals and 63% C sp^2 hybrid orbitals. Co1−O and Co1−N bonds are also with eBO of 0.9, however with a major contribution of 83% from the ligand O/N, which indicates they have a more polarized covalent bond character than that of Co1−C. Thus, the shared interaction, i.e., the covalent character, is stronger in Co1−C than Co1−O/N bond, which is reflected in the ρ_b values. Co2−O and Co2−N bonds are weaker bond than those of the Co1−O/N with eBO of 0.48, again with major contribution from the O/N ligand. This is in accord with the ρ_b value listed in Table 3 with 0.73 and 0.55 e Å^{-3} respective for Co1−O1 and Co2−O1.

Atomic Charge and d-Orbital Populations. Atomic charge is an interesting fundamental quantity; however, it is hard to quantify due to the various ways of partitioning the atoms in molecule. On the basis of the Bader's QTAIM, the atom domain is defined as partitioned by zero flux surfaces, $\nabla\vec{\rho}(r)\cdot\vec{n}(r) = 0$, where $\vec{n}(r)$ is the vector normal to the surface. Such surface is defined as the boundary of an atom. The atomic volume can be obtained within such surface; the atomic charge is therefore an integration of the electron density within the atom domain. The atomic basin of Co1 and Co2 appears in cubic shape (shown in Supporting Information, Figure S4) with an atomic volume of 7.82 and 8.42 Å^3 respectively; the atomic charge thus obtained is +1.42 and +1.35. Although the difference is small, it reflects a slightly higher atomic charge and smaller atomic volume in Co1 (Co^{III}) than those in Co2 (Co^{II}). The atomic charge obtained from MM refinement gives +1.93(2) and +1.53(3) for Co1 (Co^{III}) and Co2 (Co^{II}) ions respectively; the corresponding charges from NBO analysis are 3.15 and 2.11 (Table 5). Thus, the difference in atomic charges of Co1 and Co2 is 1 *e* in NBO analysis, but 0.4 *e* in MM; this may be attributed to the Co−C(N) π bond in Co1, but not in Co2; such π bond is not taking account in NBO analysis, where only the σ bond is assigned along Co1−C (Table 4).

Moreover, the d-orbital populations of Co atom are listed in Table 5. The total number of d electrons (MM) is 7.07 for Co1 (Co^{III}) and 7.47 for Co2 (Co^{II}). The NBO analysis also gives consistent results: where at Co1 (Co^{III}) ion, three orbitals (d_{xz}, d_{yz}, $d_{x^2-y^2}$; t_{2g} in the defined coordinates) are fully occupied, the other two (d_{xy}, d_{z^2}) are nonpopulated, yet at Co2 (Co^{II}) ion, two orbitals, d_{yz} and $d_{x^2-y^2}$, are fully occupied and three others (d_{z^2}, d_{xz}, and d_{xy}) are only singly occupied as listed in Table 4. Likewise, the differences in d-orbital populations between two cobalt ions are less in MM than that in NBO analysis. Nevertheless, both indicate that Co1 has less d electrons than those of Co2. This is as expected in Co^{III} for Co1 and Co^{II} for Co2.

Furthermore, the atomic dipole and quadrupole moments[105−107] for Co1 and Co2 derived from MM are different: with Co2 smaller in magnitude than Co1. Dipole moment is 0 and 0.66 Debye; quadrupole moment is 11.06 and 12.08 for Co2 and Co1, respectively. Detail matrices are provided in Supporting Information, Table S7.

CONCLUSION

The structure and bond characterization of the mixed-valence tri-cobalt complex is investigated via high resolution X-ray diffraction study. The atomic charge and spin state of two different cobalt ions are established through many techniques including structural analysis, magnetic property, XANES and XES and charge density analysis. All results designate that the formal atomic charge of Co1 and Co2 is close to 3+ and 2+ respectively. The spin state is confirmed by using X-ray emission and magnetic property. The charge density study also agrees that the spin states of Co1 and Co2 are at low spin (S = 0) and high spin (S = 3/2), respectively. Two cobalt ions do

Table 4. Natural Bond Orbital Analyses of Co−L Bonds

bond		eBO[a]	occ	Co/Cr	%	C/N/O	%
Co1−O1	σ	0.92	1.94	$4s4p_z3d_z^2$	17.52	$2s2p_z$	82.48
Co1−C2	σ	0.90	1.88	$4s4p_z3d_z^2$	36.79	$2s2p_z$	63.21
Co1−N4	σ	0.90	1.92	$4s4p_x4p_y3d_{xy}3d_z^2$	16.91	$2s2p_x2p_y$	83.09
Co2−O1	σ	0.48	0.98	$4s4p_x3d_{xz}3d_{x^2-y^2}3d_z^2$	11.76	$2s2p_x2p_z$	88.24
Co2−N5	σ	0.48	0.97	$4s4p_y4p_z^23d_{yz}$	11.44	$2s2p_y2p_z$	88.56
Cr−$C_{carbene}$[b]	σ	0.77	1.55			$2s2p_z$	100
	n		1.58	$3d_{yz}$	100		
	n		1.75	$3d_{xz}$	100		

[a] eBO = 1/2(occ of BO − occ of anti-BO) based on NBO analysis. [b] For [(CO)$_5$CrC(OMe)] in ref 36.

dx.doi.org/10.1021/ic401147b | Inorg. Chem. 2013, 52, 11023−11033

Table 5. The d-Orbital Population of Co1 and Co2 Obtained from MM and NBO

	MM				NBO			
	Co1	%	Co2	%	Co1	%	Co2	%
d_{z^2}	0.83(2)	12	1.28(2)	18	0	0	0.99	17
d_{xz}	1.64(2)	23	1.25(2)	18	1.95	33	0.98	17
d_{yz}	1.82(2)	26	1.75(2)	25	1.95	33	1.96	34
$d_{x^2-y^2}$	1.87(2)	26	1.88(2)	27	1.94	33	1.98	34
d_{xy}	0.91(2)	13	1.31(2)	19	0	0	0.98	17
total d-e, *e*	7.07		7.47		5.85		6.89	
atomic charge, *e*	1.93		1.53		3.15		2.11	
atomic volume, Å^3	7.82		8.42					

show apparent charge concentration and charge depletion around *i*-VSCC distribution; the unevenly distributed d-orbital populations are manifested. The topological properties at BCPs of chemical bonds indicate that Co−C bonds are polarized covalent bond with higher ρ_b and more negative H_b than those of Co−N and Co−O, while Co−O and Co−N are described as dative bonds with a small ρ_b value and near zero value in H_b. The ρ_b value is such that $Co-C_{CN} > Co-O_{OH} \geq Co-N_{trz}$. The chemical bonds of ligands, such as C−C, N−N, and C−N bonds, show typical covalent character with large ρ_b, negative $\nabla^2\rho_b$, and large negative H_b.

■ ASSOCIATED CONTENT

Supporting Information

(a) Local coordinates cobalt atoms; (b) the comparison between the XES of **1** and simulated spectra with various ratios of Co^{II}/Co^{III} and their differences; (c) the plot of the integrals of absolute value of the area difference (IAD) versus average spin values; (d) atomic basins of cobalt atoms; (e) deformation density and Laplacian distribution of C2−N2 bond; (f) molecular graph of **1**; (g) crystal data of **1**; (h) list of bond distances (Å) and angles (°); (i) differences of mean-squares displacement amplitudes (DMSDA) based on Hirshfeld rigid bond analysis; (j) list of topological properties associated with bond critical points; (k) natural bond orbital analysis of Co−L bonds; (l) list of hydrogen bonds; (m) atomic dipole and quadrupole matrices from MM. These materials are available free of charge via the Internet at http://pubs.acs.org.

■ AUTHOR INFORMATION

Corresponding Authors

*(Y.W.) Fax: (+) 886 2 23638377. E-mail: wangyu@ntu.edu.tw.

*(I.-J.H.) E-mail: ijuihsu@ntut.edu.tw.

Present Addresses

⊥(L.-C.W.) Department of Chemistry and iNANO, Aarhus University, Aarhus, Denmark.

$(T.-C.W.) SLAC Nat'l Accelerator Lab, SSRL, Menlo Park, CA, USA.

Notes

The authors declare no competing financial interest.

■ ACKNOWLEDGMENTS

The financial support from the National Science Council of Taiwan, ROC, is highly appreciated.

■ REFERENCES

(1) Robin, M. B.; Day, P. *Adv. Inorg. Chem. Radiochem.* **1967**, *10*, 248−403.

(2) Liu, T.; Dong, D.-P.; Kanegawa, S.; Kang, S.; Sato, O.; Shiota, Y.; Yoshizawa, K.; Hayami, S.; Wu, S.; He, C.; Duan, C.-Y. *Angew. Chem., Int. Ed.* **2012**, *51*, 4367−4370.

(3) Nihei, M.; Okamoto, Y.; Sekine, Y.; Hoshino, N.; Shiga, T.; Liu, I. P. C.; Oshio, H. *Angew. Chem., Int. Ed.* **2012**, *51*, 6361−6364.

(4) Lescouezec, R.; Vaissermann, J.; Ruiz-Perez, C.; Lloret, F.; Carrasco, R.; Julve, M.; Verdaguer, M.; Dromzee, Y.; Gatteschi, D.; Wernsdorfer, W. *Angew. Chem., Int. Ed.* **2003**, *42*, 1483−1486.

(5) Toma, L. M.; Lescouezec, R.; Lloret, F.; Julve, M.; Vaissermann, J.; Verdaguer, M. *Chem. Commun.* **2003**, 1850−1851.

(6) Rosseinsky, D. R.; Mortimer, R. J. *Adv. Mater.* **2001**, *13*, 783−793.

(7) Gatteschi, D. *Adv. Mater.* **1994**, *6*, 635−645.

(8) Gatteschi, D.; Sessoli, R. *Angew. Chem., Int. Ed.* **2003**, *42*, 268−297.

(9) Mishra, A.; Wernsdorfer, W.; Parsons, S.; Christou, G.; Brechin, E. K. *Chem. Commun.* **2005**, 2086−2088.

(10) Clerac, R.; Miyasaka, H.; Yamashita, M.; Coulon, C. *J. Am. Chem. Soc.* **2002**, *124*, 12837−12844.

(11) Liu, T. F.; Fu, D.; Gao, S.; Zhang, Y. Z.; Sun, H. L.; Su, G.; Liu, Y. J. *J. Am. Chem. Soc.* **2003**, *125*, 13976−13977.

(12) Kajiwara, T.; Nakano, M.; Kaneko, Y.; Takaishi, S.; Ito, T.; Yamashita, M.; Igashira-Kamiyama, A.; Nojiri, H.; Ono, Y.; Kojima, N. *J. Am. Chem. Soc.* **2005**, *127*, 10150−10151.

(13) Liu, I. P. C.; Benard, M.; Hasanov, H.; Chen, I. W. P.; Tseng, W. H.; Fu, M. D.; Rohmer, M. M.; Chen, C. H.; Lee, G. H.; Peng, S. M. *Chem.—Eur. J.* **2007**, *13*, 8667−8677.

(14) Rumberger, E. M.; Shah, S. J.; Beedle, C. C.; Zakharov, L. N.; Rheingold, A. L.; Hendrickson, D. N. *Inorg. Chem.* **2005**, *44*, 2742−2752.

(15) Sato, O.; Iyoda, T.; Fujishima, A.; Hashimoto, K. *Science* **1996**, *272*, 704−705.

(16) Bleuzen, A.; Lomenech, C.; Escax, V.; Villain, F.; Varret, F.; Moulin, C. C. D.; Verdaguer, M. *J. Am. Chem. Soc.* **2000**, *122*, 6648−6652.

(17) Champion, G.; Escax, V.; Cartier dit Moulin, C.; Bleuzen, A.; Villain, F.; Baudelet, F.; Dartyge, E.; Verdaguer, M. *J. Am. Chem. Soc.* **2001**, *123*, 12544−12546.

(18) Escax, V.; Bleuzen, A.; Cartier dit Moulin, C.; Villain, F.; Goujon, A.; Varret, F.; Verdaguer, M. *J. Am. Chem. Soc.* **2001**, *123*, 12536−12543.

(19) Moulin, C. C. D.; Villain, F.; Bleuzen, A.; Arrio, M. A.; Sainctavit, P.; Lomenech, C.; Escax, V.; Baudelet, F.; Dartyge, E.; Gallet, J. J.; Verdaguer, M. *J. Am. Chem. Soc.* **2000**, *122*, 6653−6658.

(20) Bencini, A.; Gatteschi, D.; Zanchini, C.; Haasnoot, J. G.; Prins, R.; Reedijk, J. *Inorg. Chem.* **1985**, *24*, 2812−2815.

(21) Prins, R.; Birker, P. J. M. W. L.; Haasnoot, J. G.; Verschoor, G. C.; Reedijk, J. *Inorg. Chem.* **1985**, *24*, 4128−4133.

(22) Slangen, P. M.; van Koningsbruggen, P. J.; Goubitz, K.; Haasnoot, J. G.; Reedijk, J. *Inorg. Chem.* **1994**, *33*, 1121−1126.

(23) van Koningsbruggen, P. J.; Gluth, M. W.; Ksenofontov, V.; Walcher, D.; Schollmeyer, D.; Levchenko, G.; Gutlich, P. *Inorg. Chim. Acta* **1998**, *273*, 54−61.

(24) Chuang, Y. C.; Ho, W. L.; Sheu, C. F.; Lee, G. H.; Wang, Y. *Chem. Commun.* **2012**, *48*, 10769−10771.

(25) Chuang, Y. C.; Liu, C. T.; Sheu, C. F.; Ho, W. L.; Lee, G. H.; Wang, C. C.; Wang, Y. *Inorg. Chem.* **2012**, *51*, 4663−4671.
(26) Ozarowski, A.; Yu, S. Z.; Mcgarvey, B. R.; Mislankar, A.; Drake, J. E. *Inorg. Chem.* **1991**, *30*, 3167−3174.
(27) Garcia, Y.; Kahn, O.; Rabardel, L.; Chansou, B.; Salmon, L.; Tuchagues, J. P. *Inorg. Chem.* **1999**, *38*, 4663−4670.
(28) Liu, J. C.; Xu, Y.; Duan, C. Y.; Wang, S. L.; Liao, F. L.; Zhuang, J. Z.; You, X. Z. *Inorg. Chim. Acta* **1999**, *295*, 229−233.
(29) Rat, M.; de Sousa, R. A.; Tomas, A.; Frapart, Y.; Tuchagues, J. P.; Artaud, I. *Eur. J. Inorg. Chem.* **2003**, 759−765.
(30) Stamatatos, T. C.; Bell, A.; Cooper, P.; Terzis, A.; Raptopoulou, C. P.; Heath, S. L.; Winpenny, R. E. P.; Perlepes, S. P. *Inorg. Chem. Commun.* **2005**, *8*, 533−538.
(31) Koritsanszky, T. S.; Coppens, P. *Chem. Rev.* **2001**, *101*, 1583−1627.
(32) Gatti, C. *Z. Kristallogr.* **2005**, *220*, 399−457.
(33) Coppens, P. *Angew. Chem., Int. Ed.* **2005**, *44*, 6810−6811.
(34) Farrugia, L. J.; Mallinson, P. R.; Stewart, B. *Acta Crystallogr. Sect. B* **2003**, *59*, 234−247.
(35) Overgaard, J.; Larsen, F. K.; Timco, G. A.; Iversen, B. B. *Dalton Trans.* **2009**, 664−671.
(36) Wang, C. C.; Wang, Y.; Liu, H. J.; Lin, K. J.; Chou, L. K.; Chan, K. S. *J. Phys. Chem. A* **1997**, *101*, 8887−8901.
(37) Lee, C. R.; Wang, C. C.; Chen, K. C.; Lee, G. H.; Wang, Y. *J. Phys. Chem. A* **1999**, *103*, 156−165.
(38) Wang, C. C.; Tang, T. H.; Wang, Y. *J. Phys. Chem. A* **2000**, *104*, 9566−9572.
(39) Lee, C. R.; Tan, L. Y.; Wang, Y. *J. Phys. Chem. Solids* **2001**, *62*, 1613−1628.
(40) Poulsen, R. D.; Jorgensen, M. R. V.; Overgaard, J.; Larsen, F. K.; Morgenroth, W. G.; Graber, T.; Chen, Y. S.; Iversen, B. B. *Chem.—Eur. J.* **2007**, *13*, 9775−9790.
(41) Clausen, H. F.; Overgaard, J.; Chen, Y. S.; Lversen, B. B. *J. Am. Chem. Soc.* **2008**, *130*, 7988−7996.
(42) Pillet, S.; Souhassou, M.; Mathoniere, C.; Lecomte, C. *J. Am. Chem. Soc.* **2004**, *126*, 1219−1228.
(43) Macchi, P.; Schultz, A. J.; Larsen, F. K.; Iversen, B. B. *J. Phys. Chem. A* **2001**, *105*, 9231−9242.
(44) Claiser, N.; Souhassou, M.; Lecomte, C.; Gillon, B.; Carbonera, C.; Caneschi, A.; Dei, A.; Gatteschi, D.; Bencini, A.; Pontillon, Y.; Lelievre-Berna, E. *J. Phys. Chem. B* **2005**, *109*, 2723−2732.
(45) Sparkes, H. A.; Brayshaw, S. K.; Weller, A. S.; Howard, J. A. K. *Acta Crystallogr. Sect. B* **2008**, *64*, 550−557.
(46) Jansen, G.; Schubart, M.; Findeis, B.; Gade, L. H.; Scowen, I. J.; McPartlin, M. *J. Am. Chem. Soc.* **1998**, *120*, 7239−7251.
(47) Bianchi, R.; Gervasio, G.; Marabello, D. *Inorg. Chem.* **2000**, *39*, 2360−2366.
(48) Deeken, S.; Motz, G.; Bezugly, V.; Borrmann, H.; Wagner, F. R.; Kempe, R. *Inorg. Chem.* **2006**, *45*, 9160−9162.
(49) Farrugia, L. J.; Evans, C. *C. R. Chim.* **2005**, *8*, 1566−1583.
(50) Macchi, P.; Proserpio, D. M.; Sironi, A. *J. Am. Chem. Soc.* **1998**, *120*, 13429−13435.
(51) Macchi, P.; Sironi, A. *Coord. Chem. Rev.* **2003**, *238*, 383−412.
(52) Macchi, P.; Donghi, D.; Sironi, A. *J. Am. Chem. Soc.* **2005**, *127*, 16494−16504.
(53) Overgaard, J.; Larsen, F. K.; Schiøtt, B.; Iversen, B. B. *J. Am. Chem. Soc.* **2003**, *125*, 11088−11099.
(54) Overgaard, J.; Clausen, H. F.; Platts, J. A.; Iversen, B. B. *J. Am. Chem. Soc.* **2008**, *130*, 3834−3843.
(55) Poulsen, R. D.; Overgaard, J.; Schulman, A.; Ostergaard, C.; Murillo, C. A.; Spackman, M. A.; Iversen, B. B. *J. Am. Chem. Soc.* **2009**, *131*, 7580−7591.
(56) Wu, L.-C.; Hsu, C.-W.; Chuang, Y.-C.; Lee, G.-H.; Tsai, Y.-C.; Wang, Y. *J. Phys. Chem. A* **2011**, *115*, 12602−12615.
(57) Pillet, S.; Legrand, V.; Weber, H. P.; Souhassou, M.; Letard, J. F.; Guionneau, P.; Lecomte, C. *Z. Kristallogr.* **2008**, *223*, 235−249.
(58) Fomitchev, D. V.; Furlani, T. R.; Coppens, P. *Inorg. Chem.* **1998**, *37*, 1519−1526.
(59) Bader, R. F. W. *Atoms in Molecules: A Quantum Theory*; Clarendon Press: Oxford, 1990.
(60) Hansen, N. K.; Coppens, P. *Acta Crystallogr., Sect. A* **1978**, *34*, 909−921.
(61) Coppens, P. *X-Ray Charge Densities and Chemical Bonding*, 1st ed.; Oxford University Press: Oxford, U.K., 1997.
(62) Gatti, C.; Lasi, D. *Faraday Discuss.* **2007**, *135*, 55−78.
(63) Mcweeny, R. *Rev. Mod. Phys.* **1960**, *32*, 335−369.
(64) Bader, R. F. W.; Stephens, M. E. *Chem. Phys. Lett.* **1974**, *26*, 445−449.
(65) Bader, R. F. W.; Stephens, M. E. *J. Am. Chem. Soc.* **1975**, *97*, 7391−7399.
(66) Spackman, M. A.; McKinnon, J. J. *CrystEngComm* **2002**, 378−392.
(67) McKinnon, J. J.; Jayatilaka, D.; Spackman, M. A. *Chem. Commun.* **2007**, 3814−3816.
(68) Spackman, M. A.; Jayatilaka, D. *CrystEngComm* **2009**, *11*, 19−32.
(69) Hozoi, L.; de Vries, A. H.; Broer, R. *Phys. Rev. B* **2001**, *64*, 165104.
(70) Sikora, M.; Kapusta, C.; Knížek, K.; Jirák, Z.; Autret, C.; Borowiec, M.; Oates, C. J.; Procházka, V.; Rybicki, D.; Zajac, D. *Phys. Rev. B* **2006**, *73*, 0944261.
(71) Sikora, M.; Knizek, K.; Kapusta, C.; Glatzel, P. *J. Appl. Phys.* **2008**, *103*, 07C907.
(72) de Groot, F. M. F. *Coord. Chem. Rev.* **2005**, *249*, 31−63.
(73) Glatzel, P.; Bergmann, U. *Coord. Chem. Rev.* **2005**, *249*, 65−95.
(74) Tyson, T. A.; Qian, Q.; Kao, C. C.; Rueff, J. P.; de Groot, F. M. F.; Croft, M.; Cheong, S. W.; Greenblatt, M.; Subramanian, M. A. *Phys. Rev. B* **1999**, *60*, 4665−4674.
(75) Qian, Q.; Tyson, T. A.; Kao, C. C.; Rueff, J. P.; de Groot, F. M. F.; Croft, M.; Cheong, S. W.; Greenblatt, M.; Subramanian, M. A. *J. Phys. Chem. Solids* **2000**, *61*, 457−460.
(76) Qian, Q.; Tyson, T. A.; Kao, C. C.; Croft, M.; Cheong, S. W.; Greenblatt, M. *Phys. Rev. B* **2000**, *62*, 13472−13481.
(77) Lengsdorf, R.; Rueff, J. P.; Vanko, G.; Lorenz, T.; Tjeng, L. H.; Abd-Elmeguid, M. M. *Phys. Rev. B* **2007**, *75*, 180401.
(78) Lin, J. F.; Struzhkin, V. V.; Jacobsen, S. D.; Hu, M. Y.; Chow, P.; Kung, J.; Liu, H. Z.; Mao, H. K.; Hemley, R. J. *Nature* **2005**, *436*, 377−380.
(79) Mattila, A.; Pylkkänen, T.; Rueff, J. P.; Huotari, S.; Vankó, G.; Hanfland, M.; Lehtinen, M.; Hämäläinen, K. *J. Phys.: Condens. Matter* **2007**, *19*, 386206.
(80) Vankó, G.; Neisius, T.; Molnár, G.; Renz, F.; Kárpáti, S.; Shukla, A.; de Groot, F. M. F. *J. Phys. Chem. B* **2006**, *110*, 11647−11653.
(81) Vankó, G.; Rueff, J.-P.; Mattila, A.; Németh, Z.; Shukla, A. *Phys. Rev. B* **2006**, *73*, 024424.
(82) Vankó, G.; Renz, F.; Molnár, G.; Neisius, T.; Kárpáti, S. *Angew. Chem., Int. Ed.* **2007**, *46*, 5306−5309.
(83) *CrysAlisPro System Software*, 1.171.33.34d; Oxford Diffraction Ltd.: Abingdon, England, 2009.
(84) Sheldrick, G. M. *Acta Crystallogr., Sect. A* **1990**, *46*, 467−473.
(85) *SHELXTL NT/2000, Programs for Crystal Structure Analysis*, 6.12, 2000.
(86) Volkov, P. M. A.; Farrugia, L. J.; Gatti, C.; Mallinson, P.; Richter, T.; Koritsanszky, T. *XD2006 - A Computer Program for Multipole Refinement, Topological Analysis of Charge Densities, Evaluation of Intermolecular Energies from Experimental or Theoretical Structure Factors*, 2006
(87) Clementi, E.; Raimondi, D. L. *J. Chem. Phys.* **1963**, *38*, 2686−2689.
(88) Clementi, E.; Roetti, C. *Atomic Data Nuclear Data Tables* **1974**, *14*, 177−478.
(89) Su, Z. W.; Coppens, P. *Acta Crystallogr., Sect. A* **1998**, *54*, 646−652.
(90) Birmingham, K. P. *Int. Tables X-ray Crystallogr.* **1974**, *IV*, 103−144.
(91) Steiner, T. *Angew. Chem., Int. Ed.* **2002**, *41*, 48−76.

(92) Sabino, J. R.; Coppens, P. *Acta Crystallogr., Sect. A* **2003**, *59*, 127−131.
(93) Deutsch, M.; Claiser, N.; Gillet, J. M.; Lecomte, C.; Sakiyama, H.; Tone, K.; Souhassou, M. *Acta Crystallogr. Sect. B* **2011**, *67*, 324−332.
(94) Alba, J. C. O.; Jané, C. B. *XAIM X Atoms in Molecules Interface*, version 1.0, 1998.
(95) Frisch, M. J. T., G. W.; Schlegel, H. B.; Scuseria, G. E.; Robb, M. A.; Cheeseman, J. R.; Montgomery, Jr. J. A.; Vreven, T.; Kudin, K. N.; Burant, J. C.; Millam, J. M.; Iyengar, S. S.; Tomasi, J.; Barone, V.; Mennucci, B.; Cossi, M.; Scalmani, G.; Rega, N.; Petersson, G. A.; Nakatsuji, H.; Hada, M.; Ehara, M.; Toyota, K.; Fukuda, R.; Hasegawa, J.; Ishida, M.; Nakajima, T.; Honda, Y.; Kitao, O.; Nakai, H.; Klene, M.; Li, X.; Knox, J. E.; Hratchian, H. P.; Cross, J. B.; Bakken, V.; Adamo, C.; Jaramillo, J.; Gomperts, R.; Stratmann, R. E.; Yazyev, O.; Austin, A. J.; Cammi, R.; Pomelli, C.; Ochterski, J. W.; Ayala, P. Y.; Morokuma, K.; Voth, G. A.; Salvador, P.; Dannenberg, J. J.; Zakrzewski, V. G.; Dapprich, S.; Daniels, A. D.; Strain, M. C.; Farkas, O.; Malick, D. K.; Rabuck, A. D.; Raghavachari, K.; Foresman, J. B.; Ortiz, J. V.; Cui, Q.; Baboul, A. G.; Clifford, S.; Cioslowski, J.; Stefanov, B. B.; Liu, G.; Liashenko, A.; Piskorz, P.; Komaromi, I.; Martin, R. L.; Fox, D. J.; Keith, T.; Al-Laham, M. A.; Peng, C. Y.; Nanayakkara, A.; Challacombe, M.; Gill, P. M. W.; Johnson, B.; Chen, W.; Wong, M. W.; Gonzalez, C.; Pople, J. A. *Gaussian 03, Revision C.02*, 2004.
(96) Lee, C. T.; Yang, W. T.; Parr, R. G. *Phys. Rev. B* **1988**, *37*, 785−789.
(97) Becke, A. D. *J. Chem. Phys.* **1993**, *98*, 5648−5652.
(98) Glendening, E. D.; Badenhoop, J., K.; Reed, A. E.; Carpenter, J. E.; Bohmann, J. A.; Morales, C. M.; Weinhold, F.*NBO 5.0*, 2001.
(99) Drew, M. G. B.; Harding, C. J.; Mckee, V.; Morgan, G. G.; Nelson, J. *J. Chem. Soc., Chem. Commun.* **1995**, 1035−1038.
(100) Guionneau, P.; Brigouleix, C.; Barrans, Y.; Goeta, A. E.; Letard, J. F.; Howard, J. A. K.; Gaultier, J.; Chasseau, D. *C. R. Acad. Sci. Paris, Chim./Chem.* **2001**, *4*, 161−171.
(101) Figgis, B. N. *Nature* **1958**, *182*, 1568−1570.
(102) Yamamoto, T. *X-Ray Spectrom.* **2008**, *37*, 572−584.
(103) Peng, G.; de Groot, F. M. F.; Hamalainen, K.; Moore, J. A.; Wang, X.; Grush, M. M.; Hastings, J. B.; Siddons, D. P.; Armstrong, W. H.; Mullins, O. C.; Cramer, S. P. *J. Am. Chem. Soc.* **1994**, *116*, 2914−2920.
(104) Gillespie, R. J.; Nyholm, R. S. *Q. Rev Chem Soc* **1957**, *11*, 339−380.
(105) Spackman, M. A. *Chem. Rev.* **1992**, *92*, 1769−1797.
(106) Cortés-Guzmán, F.; Bader, R. F. W. *Coord. Chem. Rev.* **2005**, *249*, 633−662.
(107) Farrugia, L. J.; Evans, C. *J. Phys. Chem. A* **2005**, *109*, 8834−8848.